Monthly Notices
of the
ROYAL ASTRONOMICAL SOCIETY

MNRAS **467,** 802–811 (2017)
Advance Access publication 2017 January 9

doi:10.1093/mnras/stx037

Discovery of the most metal-poor damped Lyman α system

Ryan J. Cooke,[1,2]★† Max Pettini[3] and Charles C. Steidel[4]

[1]*UCO/Lick Observatory, University of California, Santa Cruz, CA 95064, USA*
[2]*Department of Physics, Centre for Extragalactic Astronomy, Durham University, South Road, Durham DH1 3LE, UK*
[3]*Institute of Astronomy, Madingley Road, Cambridge CB3 0HA, UK*
[4]*California Institute of Technology, MS 249-17, Pasadena, CA 91125, USA*

Accepted 2017 January 5. Received 2016 December 15; in original form 2016 November 21

ABSTRACT

We report the discovery and analysis of the most metal-poor damped Lyman α (DLA) system currently known, based on observations made with the Keck HIRES spectrograph. The metal paucity of this system has only permitted the determination of three element abundances: $[C/H] = -3.43 \pm 0.06$, $[O/H] = -3.05 \pm 0.05$ and $[Si/H] = -3.21 \pm 0.05$, as well as an upper limit on the abundance of iron: $[Fe/H] \leq -2.81$. This DLA is among the most carbon-poor environment currently known with detectable metals. By comparing the abundance pattern of this DLA to detailed models of metal-free nucleosynthesis, we find that the chemistry of the gas is consistent with the yields of a $20.5\,M_{\odot}$ metal-free star that ended its life as a core-collapse supernova; the abundances we measure are inconsistent with the yields of pair-instability supernovae. Such a tight constraint on the mass of the progenitor Population III star is afforded by the well-determined C/O ratio, which we show depends almost monotonically on the progenitor mass when the kinetic energy of the supernova explosion is $E_{\rm exp} \gtrsim 1.5 \times 10^{51}$ erg. We find that the DLA presented here has just crossed the critical 'transition discriminant' threshold, rendering the DLA gas now suitable for low mass star formation. We also discuss the chemistry of this system in the context of recent models that suggest some of the most metal-poor DLAs are the precursors of the 'first galaxies', and are the antecedents of the ultrafaint dwarf galaxies.

Key words: stars: Population III – ISM: abundances – galaxies: dwarf – quasars: absorption lines.

1 INTRODUCTION

Almost every astrophysical environment is contaminated by the nucleosynthesis of stars. To date, only a small handful of pristine environments have been identified, including a mostly ionized cloud of gas at redshift $z \simeq 3$ that may be associated with cold flows (Fumagalli, O'Meara & Prochaska 2011), and a mostly neutral cloud of gas at redshift $z \simeq 7$ attributed to either a neutral protogalaxy or the intergalactic medium (Simcoe et al. 2012; but see Bosman & Becker 2015 for an alternative interpretation). If pockets of absolutely pristine gas still exist at redshift $z \sim 3$, there may also be some environments that were enriched *exclusively* by the first generation of stars (also called Population III, or Pop III, stars).

The nature of Pop III stars, in particular their mass spectrum, is still a matter of debate. Numerical simulations that follow the collapse of primordial material from cosmological initial conditions originally suggested that Pop III stars were predominantly very massive, with typical masses in excess of $100\,M_{\odot}$ (Bromm, Coppi & Larson 1999; Nakamura & Umemura 2001; Abel, Bryan, & Norman 2002). Modern calculations suggest a somewhat lower typical mass of the first stars, and indicate that a small multiple of Pop III stars are formed in a given minihalo (Clark, Glover & Klessen 2008; Turk, Abel & O'Shea 2009; Stacy, Greif & Bromm 2010; Stacy & Bromm 2013; Hirano et al. 2014; Stacy, Bromm & Lee 2016). Although the form of the mass function has not yet been pinned down, a general conclusion borne out of the above cosmological simulations is that the initial mass function of the first stars is top heavy, with most of the total stellar mass concentrated in stars with masses $M \gtrsim 10\,M_{\odot}$.

In principle, the mass spectrum of the first stars can be inferred observationally, by identifying the chemical fingerprint of the elements that were made during the life of a Pop III star. Finding this chemical signature is a challenging prospect, since a region must be identified that is *solely* enriched by the first stars. Dedicated surveys to find putative second generation stars in the Milky Way have identified several excellent candidates (see Frebel & Norris 2015 for a review). These searches have also uncovered a striking diversity of chemical abundance patterns, including many metal-poor stars

★E-mail: ryan.j.cooke@durham.ac.uk
†Royal Society University Research Fellow.

enhanced with light elements relative to heavy elements (collectively known as carbon-enhanced metal-poor [CEMP] stars; for an overview, see Beers & Christlieb 2005), a star with apparently no iron (Keller et al. 2014), and an almost pristine star with roughly solar-scaled chemical abundances (Caffau et al. 2011). The abundance patterns of these stars are successfully reproduced by models of Pop III stellar nucleosynthesis (Heger & Woosley 2010; Cooke & Madau 2014; Ishigaki et al. 2014; Marassi et al. 2014; Tominaga, Iwamoto & Nomoto 2014); however, there is still some flexibility in the models due to the uncertain explosion mechanism of core-collapse supernovae (see e.g. Janka 2012).

A similar quest has been undertaken to identify the chemical signature of the first stars among the most metal-poor damped Lyman α (DLA) systems (Erni et al. 2006; Pettini et al. 2008; Penprase et al. 2010; Cooke et al. 2011a,b; Cooke, Pettini & Murphy 2012). DLAs are clouds of mostly neutral gas that are observed in absorption against a bright background source, typically a quasar (for a general review of DLAs, see Wolfe, Gawiser & Prochaska 2005). DLAs are typically observed at redshift $z \simeq 3$ ($\sim$2 Gyr after the big bang), where many of the rest-frame ultraviolet absorption lines of interest are conveniently redshifted into the optical spectral range. The absorption lines associated with the most metal-poor DLAs are typically very weak, owing to the low metal abundance; in such systems, only the most abundant elements can be reliably measured with current telescope facilities (Cooke et al. 2013).

The most metal-poor DLAs are thought to be the antecedents of the lowest mass galaxies (Salvadori & Ferrara 2012; Webster, Bland-Hawthorn & Sutherland 2015; Cooke, Pettini & Jorgenson 2015), as well as cold gas streams being accreted on to galaxies (Yuan & Cen 2016). Such an affiliation marks these DLAs as a promising environment to measure – at high redshift – the chemical abundance pattern of the earliest generation of stars.

In this paper, we present the discovery of the most metal-poor DLA currently known, and discuss the chemistry of this near-pristine environment. In Section 2, we describe the details of our observations and absorption line profile fitting. We discuss the chemistry of this newly discovered DLA in Section 3, and summarize the main conclusions of our work in Section 4.

2 OBSERVATIONS AND ANALYSIS

Among the DLAs discovered by the Sloan Digital Sky Survey (SDSS; Noterdaeme et al. 2009), we first identified the extremely metal-poor DLA towards the $z_{\rm em} = 3.22$ quasar J0903+2628 (RA = $09^{\rm h}03^{\rm m}33.^{\rm s}55$, Dec. = $+26^{\circ}28'36.''3$; $m_{\rm r} = 19.0$) based on the strong, damped Ly-α absorption feature at redshift $z_{\rm abs} = 3.076$, combined with the non-detection of the strongest associated absorption lines of C, O and Si (see Pettini et al. 2008, for a description of the technique).

We observed J0903+2628 with the Keck High Resolution Spectrometer (HIRES; Vogt et al. 1994) on 2016 March 1, 2, 30 for a total exposure time of 9 $\times$ 3600 s, in seeing conditions (full width at half-maximum, FWHM $\simeq$ 0.8 arcsec) that were well-matched to the chosen slit width (0.861 arcsec; decker C1). The nominal instrument resolution of our setup is $R \simeq 49\,000$, assumed to be a Gaussian profile with an FWHM of $v_{\rm FWHM} = 6.1\,{\rm km\,s^{-1}}$. We used the blue cross-disperser to cover the wavelength range 3700–6530 Å, with small gaps near 4600 and 5600 Å, corresponding to the gaps between the detector mosaic. All frames were binned 2 $\times$ 2 during readout.

The data were processed with the MAKEE data reduction pipeline.[1] This pipeline first subtracts the detector bias level. The locations of the echelle orders are traced using an exposure of a quartz lamp through a pinhole decker (HIRES decker D5). The pixel-to-pixel variations and the blaze function were removed by dividing the science frames by an exposure of a quartz lamp through the science slit. A one-dimensional spectrum was optimally extracted from each reduced frame, and the data were finally calibrated to a vacuum and heliocentric wavelength scale. The individual spectra were resampled and combined using the UVES_POPLER code.[2] Deviant pixels and ghosts were identified by visual inspection, and masked prior to combination.

The absorption lines were analysed using the Absorption LIne Software (ALIS) package,[3] which uses the atomic data tabulated by Morton (2003). Both the quasar continuum emission and the DLA absorption lines were fit simultaneously. The quasar continuum was modelled with a low-order Legendre polynomial locally around each absorption line, while each DLA absorption component was modelled with a Voigt profile. The Lyman α (Lyα) profile of the DLA is presented in Fig. 1 (black histogram) overlaid with the best-fitting Voigt profile (red curve), corresponding to a neutral hydrogen column density of $\log N({\rm H\,I})/{\rm cm^{-2}} = 20.32 \pm 0.05$.

We detect the metal absorption lines of C II, O I and Si II, reproduced in Fig. 2, together with the best-fitting model profiles. The absorption profiles can be described by three components, located in two distinct velocity intervals. The primary absorption component is located at $z_{\rm abs} = 3.077\,588 \pm 0.000\,002$, and exhibits a turbulent Doppler parameter of $b_1 = 9.4 \pm 0.2\,{\rm km\,s^{-1}}$. The two additional 'satellite' components are located at a velocity of $\Delta v_2 \simeq -68.9\,{\rm km\,s^{-1}}$ and $\Delta v_3 \simeq -93.1\,{\rm km\,s^{-1}}$ relative to the primary component, with Doppler parameters $b_2 = 10.8 \pm 0.5\,{\rm km\,s^{-1}}$ and $b_3 = 15.9 \pm 0.7\,{\rm km\,s^{-1}}$, respectively. In addition to the turbulent broadening quoted above, we assume that the line profiles of all absorption components are thermally broadened by gas at a kinetic temperature of $T_{\rm kin} = 10^4$ K (see Cooke et al. 2015).[4] Some of the DLA absorption lines shown in Fig. 2 are mildly blended with absorption unrelated to the DLA. We simultaneously fit the DLA absorption and the unrelated absorption, and display the model profile of the unrelated blends in Fig. 2, represented by the light purple line.

The column densities of each component of the detected ions are listed in Table 1, and are mostly driven by C II λ1334, O I λ1302 and Si II λ1260. We also list a 3σ upper limit on the Fe II column density, which is based on the non-detection of Fe II λ1260, integrated over the velocity interval of Component 1. The errors on the column density measurements are computed using the diagonal terms of the covariance matrix. We do not detect any absorption originating from the higher ionization absorption lines of C IV and Si IV. In Table 1, we quote 3σ upper limits on the column density of these ions. Other high ionization absorption lines of interest (such as C III λ977 and Si III λ1206) are blended with the Lyα forest.

[1] MAKEE is available for download from: http://www.astro.caltech.edu/~tb/ipac_staff/tab/makee/index.html

[2] UVES_POPLER is maintained by Michael T. Murphy, and is available from the following url: http://astronomy.swin.edu.au/~mmurphy/UVES_popler

[3] ALIS is available for download from: https://github.com/rcooke-ast/ALIS

[4] We note that the choice of $T_{\rm kin} = 10^4$ K does not impact the derived column densities, since the thermal Doppler parameter is much narrower than the turbulent Doppler parameter and, in any case, all of the fitted absorption lines are on the linear part of the curve of growth where the derived column density is independent of the Doppler parameter.

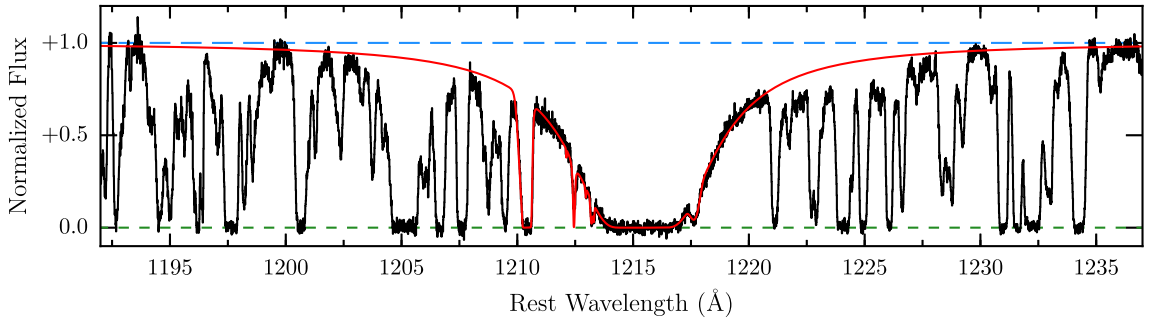

Figure 1. The H I Lyα absorption line of the DLA towards J0903+2628 at $z_{\rm abs} = 3.077\,59$ (black histogram) is shown with a Voigt profile model overlaid (red curve) corresponding to a total H I column density of $\log N({\rm H\,I})/{\rm cm}^{-2} = 20.32$. Several unrelated blends near the core of the Lyα profile are also included in the fit. The short dashed green line indicates the zero level of the data, while the long dashed blue line represents the normalized level of the quasar continuum.

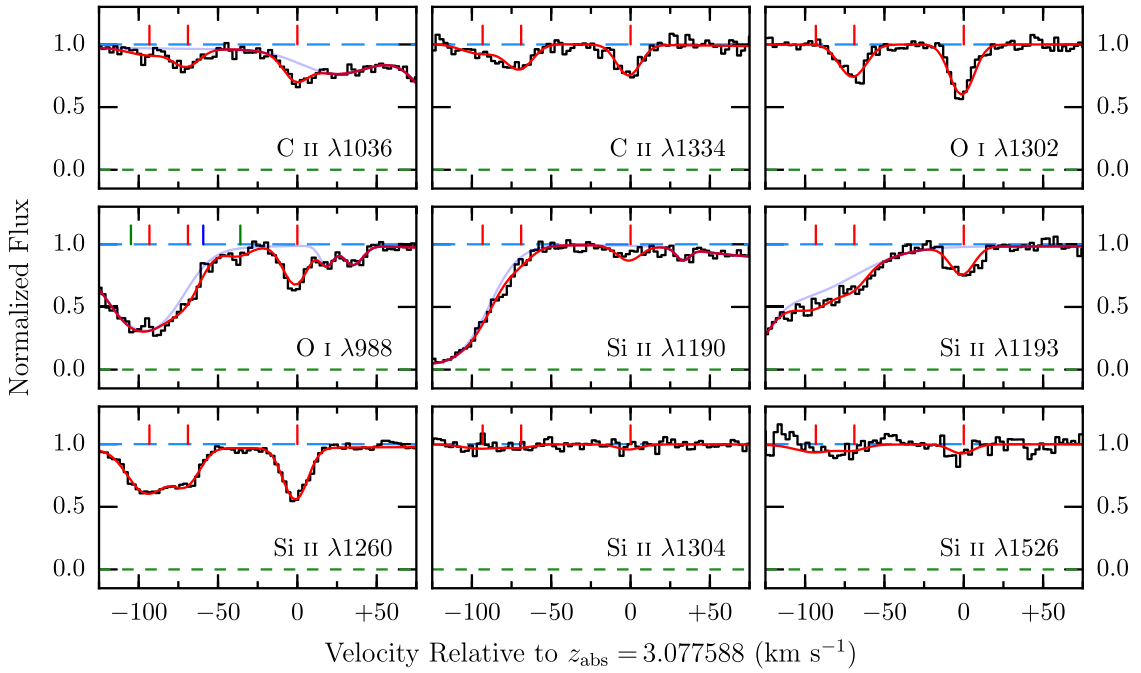

Figure 2. A selection of metal-absorption lines of the DLA towards J0903+2628 at $z_{\rm abs} = 3.077\,59$ (black histogram). In each panel, the solid red curve represents the best-fitting model profile (including fitted blends). The light purple curves shown in some of the panels represent the model profile of *just* the fitted blends (i.e. absorption that is unrelated to the DLA). The best-fitting DLA model profile consists of three components located at relative velocities $v = 0.0$, -68.9 and $-93.1\,{\rm km\,s^{-1}}$ (labelled Components 1, 2 and 3 in the text, respectively), and indicated by the red tick marks above each spectrum. The red, green and blue tick marks in the O I λ988 panel indicate the model absorption components for the O I triplet, with rest-frame wavelengths λ = 988.7734, 988.6549 and 988.5778 Å, respectively (note that one/two of the green/blue tick marks are off the plot).

Table 1. Column densities for each component of the DLA at $z_{\rm abs} = 3.077\,59$ towards J0903+2628.

X	$\log\epsilon({\rm X})_\odot$[a]	Component 1	Component 2	Component 3	Total[b]	[X/H]	[X/O]
H I	12.0	–	–	–	20.32 ± 0.05	–	–
C II	8.43	13.05 ± 0.03	12.99 ± 0.04	12.72 ± 0.08	13.32 ± 0.03	-3.43 ± 0.06	-0.38 ± 0.03
C IV	8.43	–	–	–	≤ 12.56[c]	–	–
O I	8.69	13.74 ± 0.02	13.57 ± 0.03	–	13.96 ± 0.02	-3.05 ± 0.05	–
Si II	7.51	12.40 ± 0.01	12.23 ± 0.03	12.54 ± 0.02	12.62 ± 0.01	-3.21 ± 0.05	-0.16 ± 0.02
Si IV	7.51	–	–	–	≤ 12.10[c]	–	–
Fe II	7.47	≤ 12.76	–	–	–	≤ -2.81[d]	$\leq +0.23$[e]

[a] $\log\epsilon({\rm X}) = 12 + \log N({\rm X})/N({\rm H})$. Solar values are taken from Asplund et al. (2009).
[b] The total column density only includes the components which are mostly neutral (i.e. Components 1 and 2).
[c] The upper limits on N(C IV) and N(Si IV) are integrated over the velocity interval $-100 \leq v/{\rm km\,s^{-1}} \leq +20$ relative to Component 1.
[d] The upper limit on [Fe/H] is based on the [Fe/O] limit of Component 1, combined with the total [O/H] abundance of the DLA.
[e] The [Fe/O] abundance is based only on the column densities of Component 1.

We note that Component 3 is only detected in Si II λ1260 and is marginally detected in both C II lines; this component is not observed in O I. Thus, this component may be an unfortunate blend of unrelated features, not physically associated with the DLA. However, if this component is associated with the DLA, it probably arises in a region of ionized gas, since no absorption is detected in O I. For these reasons, we consider only the column density from absorption Components 1 and 2 when assessing the relative element composition of this DLA. This ensures that we only consider the mostly neutral gas, where the observed ions are all the dominant ionization stage, thus obviating the need to perform ionization corrections.

3 RESULTS

3.1 Metal-poor chemistry

The DLA reported here is the most metal-poor system currently known, and has an oxygen abundance ([O/H] $=-3.05$) a factor of 2 lower than the next most metal-poor DLA (reported recently by Cooke et al. 2016; [O/H] $=-2.85$). Similarly, this system exhibits the lowest C and Si abundance of any known DLA. Other extremely metal-poor quasar absorption line systems are known with lower H I column density (known as Lyman limit systems, LLSs), including two systems with no detectable metals ([Z/H] $\lesssim -4.0$; Fumagalli et al. 2011) and two systems with comparable (slightly lower) metal abundances to the DLA reported here (Crighton, O'Meara & Murphy 2016; Lehner et al. 2016). Given that the abundance measurements of LLSs require an ionization correction, DLAs tend to afford somewhat higher precision abundances. This, in turn, allows for a more informative test of nucleosynthesis models.

The relative element abundances[5] of this metal-poor DLA are [C/O] $= -0.38 \pm 0.03$ and [Si/O] $= -0.16 \pm 0.02$. These abundances are somewhat lower than the typical values seen in other very metal poor DLAs (i.e. DLAs with [Fe/H] ≤ -2.0), which have [$\langle$C/O$\rangle$] $= -0.28 \pm 0.12$ and [$\langle$Si/O$\rangle$] $= -0.08 \pm 0.10$ (Cooke et al. 2011b), where the quoted uncertainty represents the 1σ spread in the very metal poor DLA population. We also find that the [Si/O] abundance is identical between Components 1 and 2, whereas the [C/O] abundance of these components differs by 0.11 dex (a 1.8σ difference). This difference is still well within the scatter of all DLA measurements (see Section 3.3).

We first compare the abundance pattern of this DLA to nucleosynthesis models of very massive metal-free stars ($M \simeq 140-260\,\mathrm{M}_\odot$) that ended their life as pair-instability supernovae (Heger & Woosley 2002). In these models, stars with a mass in this range produce element yields of $-0.66 \lesssim$ [C/O] $\lesssim -0.60$ and $+0.20 \lesssim$ [Si/O] $\lesssim +0.80$, which are inconsistent with the values we measure. It thus seems unlikely that a pair-instability supernova enriched this DLA.

We also compare the abundance pattern of this DLA to nucleosynthesis models of massive metal-free stars that ended their lives as Type II core-collapse supernovae (Heger & Woosley 2010). This set of models consists of 120 simulated stars covering a mass range $M = 10$–$100\,\mathrm{M}_\odot$, with a mass resolution of $\Delta M \gtrsim 0.1\,\mathrm{M}_\odot$. Since the explosion mechanism of a Type II supernova is still uncertain, these models adopt a parametrized 'mixing and fallback' scheme. The mixing between stellar layers during the explosion is achieved by 'smoothing' the star over the mass (i.e. radial) coordinate four times with a boxcar filter of a specified width;[6] a grid of 14 different widths is considered by Heger & Woosley (2010), where the mixing width is defined as a fraction of the He core size. Then, the explosion is simulated as a moving piston that deposits momentum at a specified mass coordinate. In what follows, we consider the standard case recommended by Heger & Woosley (2010), which places the piston near the base of the oxygen burning shell, where the entropy per baryon $S \simeq 4\,k_\mathrm{B}$, where k_B is the Boltzmann constant. The explosion is parametrized by the kinetic energy of the material that escapes the binding energy of the star, E_exp (hereafter referred to as the explosion energy). These models consider a grid of 10 values of the explosion energy for each star, in the range $(0.3-10) \times 10^{51}$ erg. Thus, this model suite comprises a total of 16 800 combinations of the three parameters: stellar mass, explosion energy and mixing width. The ranges of the model parameters discussed above are observationally motivated (see the discussion by Heger & Woosley 2010), and encompass all realistic model values.

To find the range of parameters that are an acceptable solution to the abundance pattern of the DLA reported here, we have linearly interpolated this three-dimensional space, and conducted a Markov chain Monte Carlo analysis to search for the most likely set of parameters, using the EMCEE software (Foreman-Mackey et al. 2013). In Fig. 3, we plot the one- and two-dimensional projections of the samples to identify the covariance between model parameters. (dark and light shades in the 2D projections represent the 68 and 95 per cent confidence contours, respectively). We find that the progenitor mass is well determined, centred on a value $M = 20.5\,\mathrm{M}_\odot$, while the supernova explosion energy tends towards the upper end of the range considered, with a favoured value $E_\mathrm{exp} \sim 6$–8×10^{51} erg. The mixing parameter is unconstrained.[7]

It may seem surprising that the progenitor mass of the model Population III star is so well determined relative to the other parameters of the model. This strong bound is largely due to the well-determined [C/O] value. The most abundant isotopes of C and O (i.e. ^{12}C and ^{16}O) are primarily formed by helium burning, with some ^{16}O resulting from neon burning (see e.g. Woosley & Weaver 1995). These models suggest that the [C/O] abundance is largely insensitive to the details of the explosion when $E_\mathrm{exp} \gtrsim 1.5 \times 10^{51}$ erg, and is almost uniquely dependent on the mass of the progenitor star (see top panel of Fig. 4). When the explosion energy is lower than this value, a higher fraction of ^{16}O (relative to ^{12}C) falls back on to the compact remnant, thereby causing the C/O ratio to increase (see e.g. fig. 4 of Heger & Woosley 2010). This is matched by a decrease in the Si/O ratio, since more Si falls back relative to O.

The monotonicity of the relationship between the [C/O] abundance and the progenitor mass (as well as the invariance of [C/O] with E_exp) breaks down above $\sim 35\,\mathrm{M}_\odot$, where higher C/O values are recovered by the models. We note that model stars with a mass above $\sim 35\,\mathrm{M}_\odot$ are ruled out by the measured [Si/O] abundance of the DLA reported here (see middle panel of Fig. 4).

[5] In what follows, we assume that the metals and hydrogen of this DLA are uniformly mixed. This assumption receives some support from observations of three very metal poor DLAs (Q0913+072, J1419+0829, J1558−0031) that exhibit two absorption components that share a similar metallicity and abundance pattern (see table 2 of Cooke et al. 2015; see also, Prochaska 2003).

[6] Heger & Woosley (2010) adopt this parametrization as it provides a good fit to the hard X-ray and optical light curves of SN 1987A.

[7] Since we only have two measured relative abundances to fit three model parameters, we are unable to fully constrain the best-fitting model parameters. The mixing parameter cannot be determined with the currently available data.

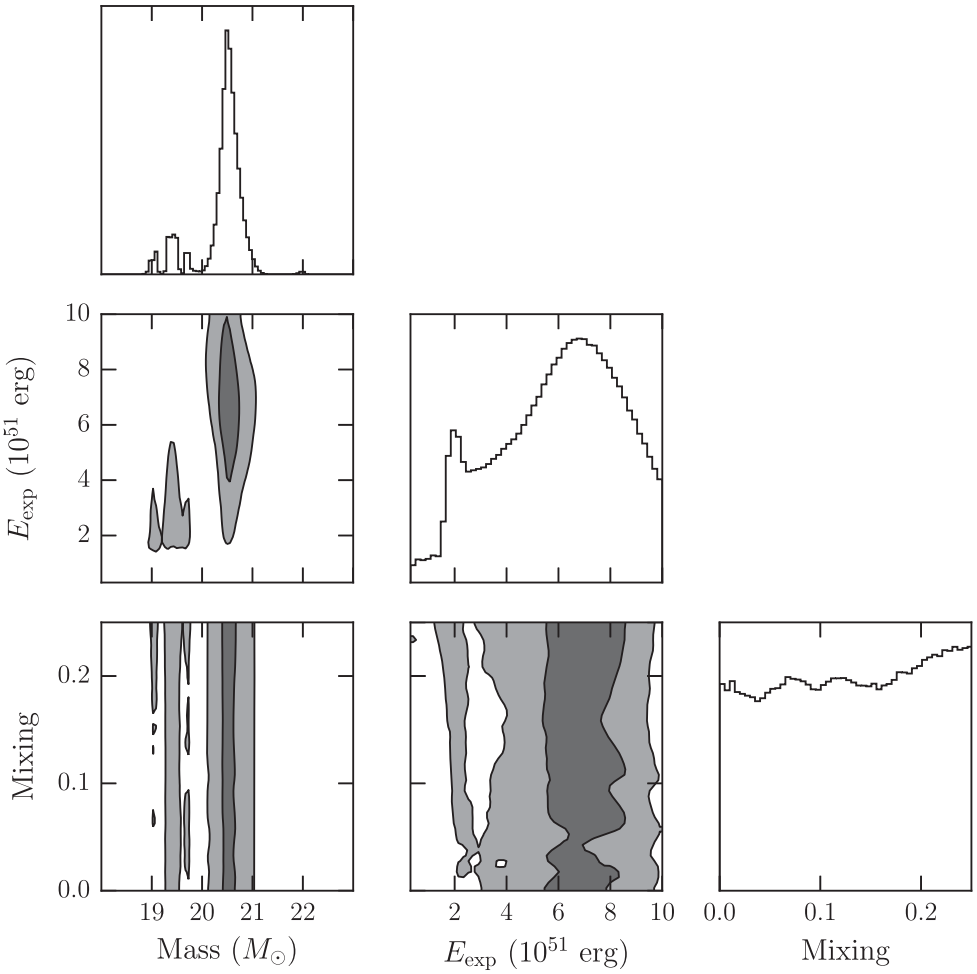

Figure 3. The observed [C/O] and [Si/O] abundances of the reported DLA have been combined with the Heger & Woosley (2010) metal-free nucleosynthesis calculations to estimate the progenitor mass, explosion energy ($E_{\rm exp}$) and stellar mixing parameter of the metal-free star that might have enriched the DLA. The diagonal panels show the marginalized probability of each model parameter shown on the x-axis. The middle left, bottom left and bottom middle panels show the two-dimensional projections, which demonstrate that the model parameters are not degenerate with one another. Dark and light shades enclose the 68 and 95 per cent confidence contours, respectively. The non-contiguous regions in the two-dimensional projections are due to small changes in the nucleosynthesis of similar mass stars; these changes are caused by slight differences in the location of the various burning shells. The current observations place a strong bound on the mass of the progenitor star, independently of the explosion energy and stellar mixing parameter (see also, Fig. 4); note that the mixing parameter is unconstrained by the current data.

Given enough data, we speculate that the strong monotonic dependence of the C/O ratio on progenitor mass might allow a robust measure of the Pop III initial mass function. The main uncertainty governing the calculated [C/O] ratio is the $^{12}{\rm C}(\alpha,\,\gamma)^{16}{\rm O}$ reaction rate that is used as input into the stellar models; the value of this rate adopted by Heger & Woosley (2010) is consistent with the latest empirical determination reported by An et al. (2016). However, we caution that other effects such as rotation (Hirschi 2007; Ekström et al. 2008; Joggerst, Woosley & Heger 2009), mass-loss via rotation/winds (Meynet & Maeder 2002) and the three-dimensional modelling of metal-free stars (Joggerst, Almgren & Woosley 2010) may alter the dependence of C/O on the progenitor mass.

The somewhat weaker bound on $E_{\rm exp}$ shown in Fig. 3 is primarily derived from the measured [Si/O] ratio (see middle panel of Fig. 4). We note that a tighter bound on the explosion energy could be afforded by the [Fe/O] ratio (bottom panel of Fig. 4). Unfortunately, the currently measured upper limit on this ratio ([Fe/O] $\leq +0.23$), is unable to provide an informative bound on $E_{\rm exp}$. Since the [Fe/O] abundance is also highly sensitive to the chosen mixing parameter, a measurement of the [Ni/Fe] abundance is needed to break the degeneracy (see Cooke et al. 2013). These measurements might become possible with the next generation of 30+ m telescope facilities (see Section 3.2).

Finally, we have only two relative element abundances with which to constrain the nucleosynthesis models, and we are unable at this stage to rule out the possibility that this system may be contaminated by other forms of nucleosynthesis, including Population II core-collapse supernovae. At a redshift of $z_{\rm abs} = 3.077\,59$, the Universe has aged by $\simeq$1.5 Gyr after the epoch of the first stars ($z \simeq 10-15$; e.g. Maio et al. 2010), and there is enough time for a second generation of stars to have already operated in this DLA. It is nevertheless encouraging that the chemistry of this one DLA is in good agreement with the chemistry of absorption line systems at $z_{\rm abs} \simeq 6$ (Becker et al. 2012), which are captured only a few hundred Myr after the putative epoch of the first stars. It is also worth noting that the low metallicity of this DLA is consistent with the metallicity regime expected for gas that is enriched solely by metal-free Population III stars (Smith & Sigurdsson 2007; Bromm

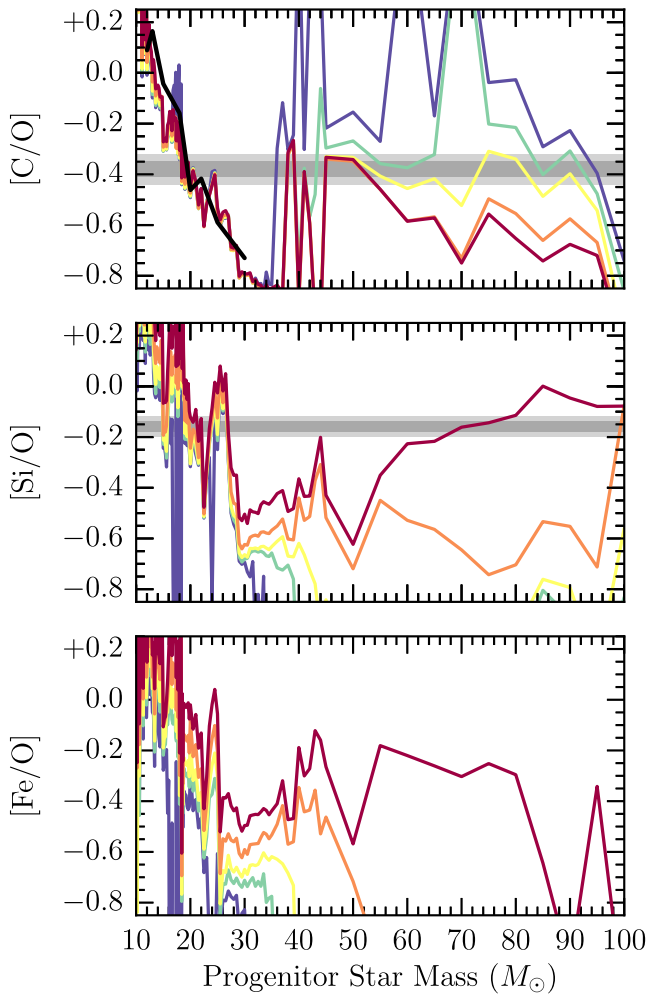

Figure 4. The calculated relative abundances of [C/O], [Si/O] and [Fe/O] of metal-free stars (Heger & Woosley 2010) are shown as a function of the progenitor star mass. Each curve is colour-coded by the kinetic energy released by the supernova explosion (blue → red = 1.8, 2.4, 3, 5, 10 × 10^{51} erg). The black curve in the top panel shows the relationship between C/O and progenitor star mass for stars with a metallicity $Z = 10^{-4}\,Z_\odot$ (Woosley & Weaver 1995). The grey shaded regions in the top and middle panels show the abundance measurements of the DLA reported here (dark and light shades represent the 68 and 95 per cent confidence bounds, respectively).

& Yoshida 2011; Wise et al. 2012; Cooke & Madau 2014; Webster et al. 2015; Ritter et al. 2016).

3.2 The antecedents of metal-poor stars and the ultrafaint dwarf galaxies

According to the Stellar Abundances for Galactic Archaeology (SAGA) data base[8] (Suda et al. 2008), the only star currently known with a lower [C/H] abundance than the DLA reported here is the Leo star (Caffau et al. 2011). The remaining stars in the SAGA data base are either red giant branch stars[9] or display a higher surface abundance of [C/H]. The star with the closest abundances to the DLA we report here is SDSS J0259+0057 (Aoki et al. 2013), which has a carbon abundance [C/H] = −3.33 ± 0.22, and is not carbon-enhanced ([C/Fe] = −0.02 ± 0.22).

If the DLA we consider here has a chemical abundance pattern that is similar to the Milky Way halo star SDSS J0259+0057, we estimate that the Fe abundance of the DLA would be [Fe/H] ≃ −3.4. The Fe abundance of the DLA can also be estimated by subtracting the typical Si/Fe abundance of very metal poor DLAs ([Si/Fe] = +0.32 ± 0.09; Cooke et al. 2011b) from the observed [Si/H] abundance, which would give [Fe/H] ≃ −3.5. We note, however, that the [Fe/H] abundance of this DLA may be considerably lower than these estimates; there exist some Milky Way halo stars with slightly higher [C/H] that exhibit a strong overabundance of [C/Fe], collectively known as CEMP stars (see e.g. Beers & Christlieb 2005). Measuring the detailed chemical abundance pattern of this DLA (including the abundances of N, Mg, Al and Fe) will become feasible with the next generation of 30+ m telescope facilities. Assuming that the abundances of these elements are in the same proportions as a typical very metal poor DLA (see table 13 of Cooke et al. 2011b), this goal could be achieved with a spectrum of S/N ≃ 150.[10]

As stated above, there is only one star currently known that is more carbon-poor than the DLA reported here. We now speculate how many DLAs might need to be observed before a DLA with an abundance as low as the Leo star may be found. The SAGA data base lists seven stars with a carbon abundance [C/H] ≤ −3.0, including the Leo star that has an abundance [C/H] ≤ −3.8. There are currently four DLAs with a carbon abundance [C/H] ≤ −3.0 (see Section 3.3 and Table 2); thus, doubling the number of DLAs

Table 2. Compilation of DLA C/O and O/H measurements.

QSO	z_{abs}	[C/O]	[O/H]	Reference[a]
J0035−0918	2.340 10	0.08 ± 0.16	−2.44 ± 0.07	1,2
HS0105+1619	2.536 51	0.110 ± 0.045	−1.776 ± 0.021	3
J0140−0839	3.696 60	−0.30 ± 0.08	−2.75 ± 0.15	4
J0311−1722	3.734 00	−0.42 ± 0.11	−2.29 ± 0.10	5
J0903+2628	3.077 59	−0.38 ± 0.03	−3.05 ± 0.05	6
Q0913+072	2.618 29	−0.36 ± 0.012	−2.416 ± 0.011	3, 7
J0953−0504	4.202 87	−0.50 ± 0.03	−2.55 ± 0.10	2
J1001+0343	3.078 41	−0.41 ± 0.03	−2.65 ± 0.05	5
J1016+4040	2.816 33	−0.21 ± 0.05	−2.46 ± 0.11	7
Q1111+1332	2.270 94	−0.18 ± 0.11	−1.92 ± 0.08	1
Q1202+3235	4.977 00	−0.33 ± 0.11	−2.02 ± 0.13	8
J1337+3153	3.167 68	−0.19 ± 0.11	−2.67 ± 0.18	9
J1358+6522	3.067 30	−0.27 ± 0.06	−2.335 ± 0.02	3, 10
J1558+4053	2.553 32	−0.06 ± 0.07	−2.45 ± 0.06	7
Q2206−199	2.076 24	−0.38 ± 0.04	−2.07 ± 0.05	7
J2155+1358	4.212 44	−0.29 ± 0.08	−1.80 ± 0.11	11

[a]1: Cooke et al. (2015); 2: Dutta et al. (2014); 3: Cooke et al. (2014); 4: Ellison et al. (2010); 5: Cooke et al. (2011b); 6: This work; 7: Pettini et al. (2008); 8: Morrison et al. (2016); 9: Srianand et al. (2010); 10: Cooke et al. (2012); 11: Dessauges-Zavadsky et al. (2003).

[8] The SAGA data base is maintained by Takuma Suda, Yutaka Katsuta and Shimako Yamada, and is available at the following address: http://sagadatabase.jp/wiki/doku.php

[9] As a star ascends the red giant branch (RGB), gas that has been processed through the CN cycle is mixed to the stellar surface, reducing the surface abundance of C (e.g. Gratton et al. 2000). As a result, the [C/H] abundance that an upper RGB star was born with can only be recovered by applying a correction based on stellar evolution models (Placco et al. 2014). After correcting for this effect, Placco et al. (2014) find ∼10 RGB stars that exhibit a corrected [C/H] value that is lower than the DLA we report here.

[10] The next detectable elements include S and Ni, which would require a S/N ≃ 600 and 2000, respectively, to detect an individual absorption line at 5σ confidence. Stacking the available Ni II lines (see Cooke et al. 2013) could reduce this requirement to a S/N ≃ 1000.

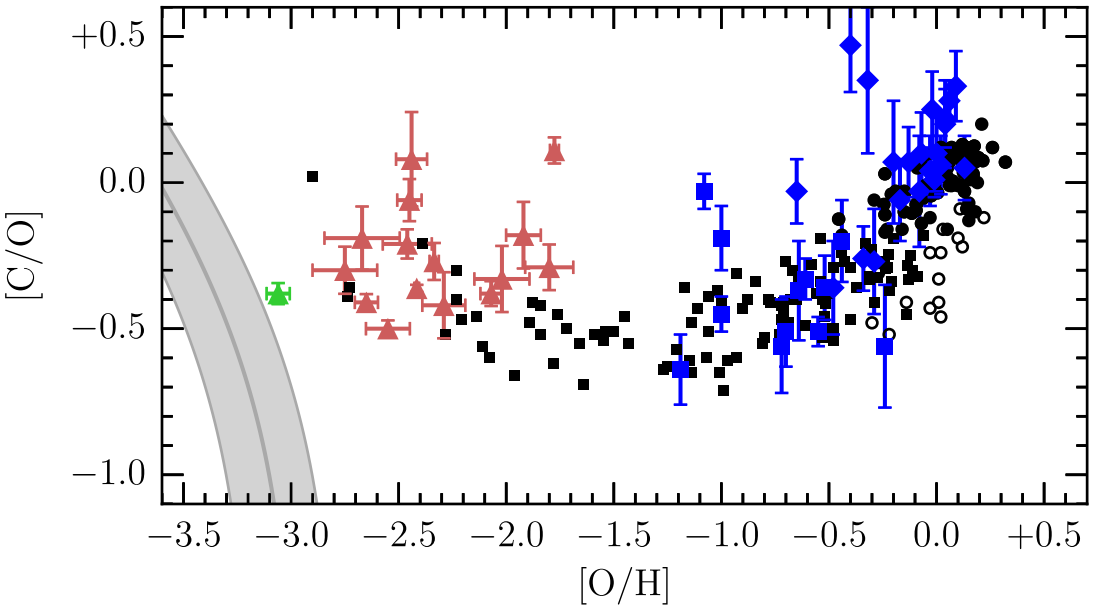

Figure 5. The chemical evolution of [C/O] is shown for various astrophysical environments. The black symbols represent stars that are kinematically associated with the thin disc (solid circles), thick disc (open circles) and halo stars (squares). The blue symbols are for H II regions, measured from optical recombination lines (diamonds) or ultraviolet collisionally excited lines (squares). The red triangles show literature measurements of [C/O] and [O/H] of metal-poor DLAs (see Table 2). The green triangle is the new measurement reported herein. The grey band represents the 'transition discriminant' proposed by Frebel, Johnson & Bromm (2007), where the width of the band indicates the uncertainty of this zone. Gas clouds to the left of this zone are not expected to form a low mass (i.e. long-lived) generation of stars. See the text for the references to all plotted data sets.

in this extremely metal-poor regime may be sufficient to uncover a DLA of similar metallicity to the Leo star.

Given the metal paucity of the DLA reported here, it is conceivable that just a *single* (Population III) star is responsible for the metal enrichment. Indeed, hydrodynamic models that trace the internal feedback[11] within idealized dwarf galaxies, do entertain this idea (Bland-Hawthorn, Sutherland & Webster 2015; Webster et al. 2015). In this scenario, the DLA reported here would be considered an immediate progenitor of a 'first galaxy' that is poised to form its first generation of low mass stars (see also, Section 3.3). This scenario receives some support from abundance measurements of stars in the lowest luminosity and most metal poor galaxies in the Local Group – the so-called ultrafaint dwarf galaxies (UFDs; Kirby et al. 2008; Norris et al. 2010; Lai et al. 2011; Simon et al. 2011; Vargas et al. 2013; Brown et al. 2014); the presumed [Fe/H] abundance of the DLA reported here ([Fe/H] $\simeq -3.5$) is comparable to the *most* Fe-poor stars in the UFDs.[12]

3.3 Metallicity evolution of the C/O ratio

We now extend this discussion to the metallicity evolution of the C/O ratio. In Fig. 5, we present the latest complement of C/O and O/H measurements available in the literature. These include abundance measurements of stars (Bensby & Feltzing 2006; Fabbian et al. 2009; Nissen et al. 2014) in the Milky Way thin and thick disc (solid and open black circles, respectively) and in the Milky Way halo (black squares). To this we add C/O measurements of local H II regions (Dufour, Shields & Talbot 1982; Garnett et al. 1995; Kurt et al. 1999; Esteban et al. 2002, 2009, 2014; García-Rojas & Esteban 2007; López-Sánchez et al. 2007; Berg et al. 2016), using either optical recombination lines or ultraviolet collisionally excited lines (blue diamonds and squares respectively).[13] Finally, we overplot measurements of C/O and O/H in the lowest metallicity DLAs (red triangles) and in the new DLA reported here (green triangle). For convenience, in Table 2, we provide all of the DLA measurements used in this work, scaled to our adopted solar abundance scale (Asplund et al. 2009, see also the second column of Table 1).

All of the observations displayed in Fig. 5 are generally in good mutual agreement, regardless of the different environments probed and the different techniques used. There are, however, a few DLAs and H II regions that exhibit somewhat enhanced C/O values relative to the locus defined by Milky Way stars. Similar enhancements have also been seen in the [C/α] ratios measured in some Lyman Limit Systems (Lehner et al. 2016; see also, Lehner et al. 2013). The origin of such enhancements is unclear at present, but could be related to the production of C by intermediate mass stars (Sharma et al. 2016).

As discussed previously in the literature (Carigi 2000; Henry, Edmunds & Köppen 2000; Akerman et al. 2004; Cescutti et al. 2009; Romano et al. 2010), the increase of [C/O] when [O/H] $\gtrsim -1.0$ is thought to be due to the metallicity-dependent winds of massive stars combined with the delayed release of C from low and intermediate mass stars. The upturn of [C/O] when [O/H] $\lesssim -1.5$, on the other hand, is still open to debate. Akerman et al. (2004, see also, Carigi & Peimbert 2011) propose that the increased C/O values seen at low O/H are the result of an increased carbon yield from metal-free Population III stars. This scenario has previously been used to explain the lowest metallicity population of

[11] Including both radiative feedback from massive stars and the subsequent supernova feedback.

[12] We note that a direct comparison between the [Si/H] abundance of this DLA and the stars in UFDs is not possible, since [Si/H] has not been measured for the *most* Fe-poor stars in UFDs (Vargas et al. 2013).

[13] We apply a correction of +0.24 dex to the [O/H] abundance measured using collisionally excited lines (Esteban et al. 2014; Steidel et al. 2016).

CEMP stars (Umeda & Nomoto 2003; Ryan et al. 2005; Cooke & Madau 2014).

In addition to the C/O upturn at low O/H, we also draw attention to the scatter in the DLA [C/O] measurements. With the improved statistics of the data collected in Table 2, we now see that the DLA values of [C/O] at a given [O/H] differ by more than their errors, suggesting an intrinsic dispersion in these elements relative abundances that was not immediately apparent in our earlier studies of carbon and oxygen in very metal poor DLAs (Pettini et al. 2008; Cooke et al. 2011b). The total range in [C/O] exhibited by DLAs with [O/H] $\lesssim -2.0$ spans a factor of $\sim$4, from [C/O] $\simeq -0.5$ to $\simeq +0.1$. There are several possibilities that could explain such a scatter. As shown in the top panel of Fig. 4 (see also, Section 3.1), the [C/O] ratio is sensitive to the mass of the stars that enriched the DLAs. If the first stars formed in isolation or in small multiples, as in currently favoured scenarios (Clark et al. 2008; Turk et al. 2009; Stacy et al. 2010; Stacy & Bromm 2013; Hirano et al. 2014; Stacy et al. 2016), the intrinsic C/O scatter could be explained if these DLAs were enriched by a single or a small multiple of Pop III stars. The predicted mass range of the stars responsible for the enrichment of these metal-poor DLAs is $10 \lesssim M/\mathrm{M}_{\odot} \lesssim 25$, with a bias towards higher mass stars. An alternative possibility, suggested recently by Sharma et al. (2016), is that the C/O scatter is due to enrichment by a combination of massive and intermediate mass (Population II) stars; the high C/O values are the result of preferential enrichment by intermediate mass stars while the low C/O values are primarily due to massive stars. The observed C/O scatter is the result of poor mixing between these two channels of carbon production.

We point out that massive Population II stars alone are less likely to produce the observed C/O scatter than Population III stars, even though the relationship between C/O and progenitor star mass is nearly identical for Population III stars and stars with progenitor metallicity $Z = 10^{-4}Z_{\odot}$ (see the black curve in the top panel of Fig. 4). This is because the stellar initial mass function of Population II stars is more fully sampled (therefore yielding an IMF-weighted C/O ratio), unlike the sparsely sampled initial mass function of Population III stars, as discussed above. For these reasons, we suggest that the distribution of C/O measurements in the most metal-poor DLAs might provide a measure of both the stellar initial mass function and multiplicity of the first stars. Measuring the intrinsic scatter of C/O in almost pristine environments should be considered a key goal of future observations.

In Fig. 5, we also overlay the 'transition discriminant' (Frebel et al. 2007, see also Bromm & Loeb 2003), shown by the solid grey shaded region, which marks the transition from a predominantly high mass generation of (Population III) stars to a low mass generation of (Population II) stars. This criterion is based on the fine structure cooling lines of [C II] and [O I]. Once a critical abundance of C and O is reached in a cloud of cold neutral gas (i.e. to the right of the grey band shown in Fig. 5), the gas is able to fragment to low mass scales and produce a long-lived generation of stars. In principle, DLAs are not restricted to the right of this region; a DLA that overlaps this region would be an ideal environment to empirically study the transition from Population III to Population II star formation. The DLA reported here lies very close to this region,[14] and appears to have just crossed the threshold for low mass star formation.

[14] The DLA reported here exhibits a value of the transition discriminant, $D_{\mathrm{trans}} = -3.19 \pm 0.04$, which lies just above the critical value calculated by Frebel et al. (2007), $D_{\mathrm{trans,\,crit}} = -3.5 \pm 0.2$.

Finally, given that: (1) The gas in DLAs is mostly neutral (i.e. conducive to star formation); (2) this particular DLA has just crossed into a chemical regime where a generation of long-lived stars is expected to form and (3) the presumed [Fe/H] abundance of the DLA reported here is consistent with the *most* Fe-poor stars seen in UFDs, we suggest that this DLA could be representative of one of the antecedents of the UFD galaxy population, as discussed previously in Section 3.2.

4 SUMMARY AND CONCLUSIONS

We report the discovery of the most metal-poor DLA system currently known, located at a redshift $z_{\mathrm{abs}} = 3.077\,59$, based on observations of the quasar J0903+2628 taken with the Keck HIRES spectrograph. This DLA was identified as part of our ongoing programme to search for the nucleosynthetic imprints of the first stars in neutral gas at high redshift. We draw the following main conclusions.

(i) The extremely low metallicity of this DLA has allowed only the most abundant chemical elements to be detected. Based on Voigt profile fitting, we deduce the following abundances: [C/H] $= -3.43 \pm 0.06$, [O/H] $= -3.05 \pm 0.05$ and [Si/H] $= -3.21 \pm 0.05$, and an upper limit on the iron abundance of [Fe/H] ≤ -2.81. This DLA is a factor of $\sim$2 more oxygen-poor than the next most metal-poor DLA known (Cooke et al. 2016; [O/H] $= -2.85$).

(ii) This DLA exhibits an abundance of carbon that is lower than any metal-poor star currently known, other than the Leo star (Caffau et al. 2011). The low metallicity is consistent with the view that this DLA may have been enriched solely by the products of a first generation of stars.

(iii) We have compared the relative chemical abundances of this DLA to nucleosynthesis calculations of massive metal-free stars that ended their lives as core-collapse supernovae. We show that the C/O yield of massive metal-free stars is a strong (almost monotonic) function of the progenitor mass, and is virtually independent of the other parameters in the nucleosynthesis modelling when the explosion energy is $E_{\mathrm{exp}} \gtrsim 1.5 \times 10^{51}$erg. Using these models, we estimate that the DLA was enriched by a star of mass $M \simeq 20.5\,\mathrm{M}_{\odot}$. We also rule out the possibility that the enrichment was due to a star that ended its life as a pair-instability supernova.

(iv) The carbon and oxygen abundances of this DLA yield a measure of the transition discriminant, $D_{\mathrm{trans}} = -3.19 \pm 0.04$, which is just over the critical threshold for low mass star formation $D_{\mathrm{trans,\,crit}} = -3.5 \pm 0.2$ (Frebel et al. 2007). Given the large column density of neutral gas hosted by the DLA, which may be conducive to star formation, we propose that this environment might represent an immediate precursor to the formation of a 'first galaxy' (i.e. a dark matter halo that has not yet formed a generation of long-lived, low mass stars).

(v) We compile all available literature determinations of the C/O abundance in very metal poor DLAs. The scatter of these measurements is larger than the measurement uncertainties, indicating that there is an intrinsic dispersion in the population. Given the sensitivity of the C/O ratio to progenitor mass, we propose that the scatter can be explained if a single or small multiple of metal-free stars is responsible for the enrichment of extremely metal-poor DLAs. We also propose that the distribution of C/O measurements of extremely metal-poor DLAs can be used to determine both the stellar initial mass function and the multiplicity of the first stars.

(vi) Recent numerical models have also suggested that the most metal-poor DLAs may have been enriched by just a single massive

star, and could have similar properties to the progenitors of the Milky Way UFDs (Salvadori & Ferrara 2012; Webster et al. 2015). We note that the presumed [Fe/H] of the DLA reported here is consistent with the *most* Fe-poor stars found in the UFD galaxies. A key goal of future work will be to pin down the iron abundance of the DLA reported here and of other extremely metal-poor DLAs.

Our work highlights the importance of identifying and measuring the detailed chemical abundance patterns of the most metal-poor DLAs. The high precision and accuracy that can be achieved for the relative chemical abundances ($\lesssim$0.05 dex), allow for a strong and informative test of nucleosynthesis models of metal-free stars. In particular, the C/O ratio offers a sensitive conversion to the progenitor mass of the metal-free stars that may have enriched the most metal-poor DLAs. With future telescope facilities, it may also be possible to measure the [Ni/Fe] ratio to comparable precision, thereby allowing a strong bound on the supernova explosion energy (Cooke et al. 2013). Finally, we estimate that by merely doubling the number of DLAs with a carbon abundance [C/H] ≤ -3.0 (from 4 to 8 DLAs), it is statistically possible to find a DLA that is as carbon-poor as the Leo star. Furthermore, the future prospect of finding extremely metal-poor (and possibly, pristine) DLAs at high redshift is very promising; the steep slope of the quasar luminosity function combined with the collecting area of the 30+ m telescopes, will ensure access to $\sim$100 times more quasars than those that are within reach of current facilities (see the discussion by Cooke et al. 2016).

ACKNOWLEDGEMENTS

We are grateful to the staff astronomers at Keck Observatory for their assistance with the observations. We thank the anonymous referee for their prompt review, and for offering several helpful suggestions that improved the presentation of this paper. During this work, RJC was supported by a Royal Society University Research Fellowship, and by NASA through Hubble Fellowship grant HST-HF-51338.001-A, awarded by the Space Telescope Science Institute, which is operated by the Association of Universities for Research in Astronomy, Inc., for NASA, under contract NAS5-26555. RJC acknowledges support from STFC (ST/L00075X/1). CCS has been supported by grant AST-1313472 from the US NSF. This research was also supported by a NASA Keck PI Data Award, administered by the NASA Exoplanet Science Institute. Data presented herein were obtained at the W. M. Keck Observatory from telescope time partially allocated to the National Aeronautics and Space Administration through the agency's scientific partnership with the California Institute of Technology and the University of California. Our work made use of the MATPLOTLIB (Hunter 2007), EMCEE (Foreman-Mackey et al. 2013) and CORNER (Foreman-Mackey et al. 2016) PYTHON packages, which we gratefully acknowledge. The Observatory was made possible by the generous financial support of the W. M. Keck Foundation. We thank the Hawaiian people for the opportunity to observe from Mauna Kea; without their hospitality, this work would not have been possible.

REFERENCES

Abel T., Bryan G. L., Norman M. L., 2002, Science, 295, 93
Akerman C. J., Carigi L., Nissen P. E., Pettini M., Asplund M., 2004, A&A, 414, 931
An Z.-D., Ma Y.-G., Fan G.-T., Li Y.-J., Chen Z.-P., Sun Y.-Y., 2016, ApJ, 817, L5
Aoki W. et al., 2013, AJ, 145, 13
Asplund M., Grevesse N., Sauval A. J., Scott P., 2009, ARA&A, 47, 481
Becker G. D., Sargent W. L. W., Rauch M., Carswell R. F., 2012, ApJ, 744, 91
Beers T. C., Christlieb N., 2005, ARA&A, 43, 531
Bensby T., Feltzing S., 2006, MNRAS, 367, 1181
Berg D. A., Skillman E. D., Henry R. B. C., Erb D. K., Carigi L., 2016, ApJ, 827, 126
Bland-Hawthorn J., Sutherland R., Webster D., 2015, ApJ, 807, 154
Bosman S. E. I., Becker G. D., 2015, MNRAS, 452, 1105
Bromm V., Loeb A., 2003, Nature, 425, 812
Bromm V., Yoshida N., 2011, ARA&A, 49, 373
Bromm V., Coppi P. S., Larson R. B., 1999, ApJ, 527, L5
Brown T. M. et al., 2014, ApJ, 796, 91
Caffau E. et al., 2011, Nature, 477, 67
Carigi L., 2000, Rev. Mex. Astron. Astrofis., 36, 171
Carigi L., Peimbert M., 2011, Rev. Mex. Astron. Astrofis., 47, 139
Cescutti G., Matteucci F., McWilliam A., Chiappini C., 2009, A&A, 505, 605
Clark P. C., Glover S. C. O., Klessen R. S., 2008, ApJ, 672, 757
Cooke R. J., Madau P., 2014, ApJ, 791, 116
Cooke R., Pettini M., Steidel C. C., Rudie G. C., Jorgenson R. A., 2011a, MNRAS, 412, 1047
Cooke R., Pettini M., Steidel C. C., Rudie G. C., Nissen P. E., 2011b, MNRAS, 417, 1534
Cooke R., Pettini M., Murphy M. T., 2012, MNRAS, 425, 347
Cooke R., Pettini M., Jorgenson R. A., Murphy M. T., Rudie G. C., Steidel C. C., 2013, MNRAS, 431, 1625
Cooke R. J., Pettini M., Jorgenson R. A., Murphy M. T., Steidel C. C., 2014, ApJ, 781, 31
Cooke R. J., Pettini M., Jorgenson R. A., 2015, ApJ, 800, 12
Cooke R. J., Pettini M., Nollett K. M., Jorgenson R., 2016, ApJ, 830, 148
Crighton N. H. M., O'Meara J. M., Murphy M. T., 2016, MNRAS, 457, L44
Dessauges-Zavadsky M., Péroux C., Kim T.-S., D'Odorico S., McMahon R. G., 2003, MNRAS, 345, 447
Dufour R. J., Shields G. A., Talbot R. J., Jr, 1982, ApJ, 252, 461
Dutta R., Srianand R., Rahmani H., Petitjean P., Noterdaeme P., Ledoux C., 2014, MNRAS, 440, 307
Ekström S., Meynet G., Chiappini C., Hirschi R., Maeder A., 2008, A&A, 489, 685
Ellison S. L., Prochaska J. X., Hennawi J., Lopez S., Usher C., Wolfe A. M., Russell D. M., Benn C. R., 2010, MNRAS, 406, 1435
Erni P., Richter P., Ledoux C., Petitjean P., 2006, A&A, 451, 19
Esteban C., Peimbert M., Torres-Peimbert S., Rodríguez M., 2002, ApJ, 581, 241
Esteban C., Bresolin F., Peimbert M., García-Rojas J., Peimbert A., Mesa-Delgado A., 2009, ApJ, 700, 654
Esteban C., García-Rojas J., Carigi L., Peimbert M., Bresolin F., López-Sánchez A. R., Mesa-Delgado A., 2014, MNRAS, 443, 624
Fabbian D., Nissen P. E., Asplund M., Pettini M., Akerman C., 2009, A&A, 500, 1143
Foreman-Mackey D., 2016, J. Open Source Softw., 24
Foreman-Mackey D., Hogg D. W., Lang D., Goodman J., 2013, PASP, 125, 306
Frebel A., Norris J. E., 2015, ARA&A, 53, 631
Frebel A., Johnson J. L., Bromm V., 2007, MNRAS, 380, L40
Fumagalli M., O'Meara J. M., Prochaska J. X., 2011, Science, 334, 1245
García-Rojas J., Esteban C., 2007, ApJ, 670, 457
Garnett D. R., Skillman E. D., Dufour R. J., Peimbert M., Torres-Peimbert S., Terlevich R., Terlevich E., Shields G. A., 1995, ApJ, 443, 64
Gratton R. G., Sneden C., Carretta E., Bragaglia A., 2000, A&A, 354, 169
Heger A., Woosley S. E., 2002, ApJ, 567, 532
Heger A., Woosley S. E., 2010, ApJ, 724, 341
Henry R. B. C., Edmunds M. G., Köppen J., 2000, ApJ, 541, 660
Hirano S., Hosokawa T., Yoshida N., Umeda H., Omukai K., Chiaki G., Yorke H. W., 2014, ApJ, 781, 60
Hirschi R., 2007, A&A, 461, 571
Hunter J. D., 2007, Comput. Sci. Eng., 9, 90
Ishigaki M. N., Tominaga N., Kobayashi C., Nomoto K., 2014, ApJ, 792, L32

Janka H.-T., 2012, Annu. Rev. Nucl. Part. Sci. , 62, 407
Joggerst C. C., Woosley S. E., Heger A., 2009, ApJ, 693, 1780
Joggerst C. C., Almgren A., Woosley S. E., 2010, ApJ, 723, 353
Keller S. C. et al., 2014, Nature, 506, 463
Kirby E. N., Simon J. D., Geha M., Guhathakurta P., Frebel A., 2008, ApJ, 685, L43
Kurt C. M., Dufour R. J., Garnett D. R., Skillman E. D., Mathis J. S., Peimbert M., Torres-Peimbert S., Ruiz M.-T., 1999, ApJ, 518, 246
Lai D. K., Lee Y. S., Bolte M., Lucatello S., Beers T. C., Johnson J. A., Sivarani T., Rockosi C. M., 2011, ApJ, 738, 51
Lehner N. et al., 2013, ApJ, 770, 138
Lehner N., O'Meara J. M., Howk J. C., Prochaska J. X., Fumagalli M., 2016, ApJ, 833, 283
Limongi M., Chieffi A., 2012, ApJS, 199, 38
López-Sánchez Á. R., Esteban C., García-Rojas J., Peimbert M., Rodríguez M., 2007, ApJ, 656, 168
Maio U., Ciardi B., Dolag K., Tornatore L., Khochfar S., 2010, MNRAS, 407, 1003
Marassi S., Chiaki G., Schneider R., Limongi M., Omukai K., Nozawa T., Chieffi A., Yoshida N., 2014, ApJ, 794, 100
Meynet G., Maeder A., 2002, A&A, 390, 561
Morrison S., Kulkarni V. P., Som D., DeMarcy B., Quiret S., Péroux C., 2016, ApJ, 830, 158
Morton D. C., 2003, ApJS, 149, 205
Nakamura F., Umemura M., 2001, ApJ, 548, 19
Nissen P. E., Chen Y. Q., Carigi L., Schuster W. J., Zhao G., 2014, A&A, 568, A25
Norris J. E., Wyse R. F. G., Gilmore G., Yong D., Frebel A., Wilkinson M. I., Belokurov V., Zucker D. B., 2010, ApJ, 723, 1632
Noterdaeme P., Petitjean P., Ledoux C., Srianand R., 2009, A&A, 505, 1087
Penprase B. E., Prochaska J. X., Sargent W. L. W., Toro-Martinez I., Beeler D. J., 2010, ApJ, 721, 1
Pettini M., Zych B. J., Steidel C. C., Chaffee F. H., 2008, MNRAS, 385, 2011
Placco V. M., Frebel A., Beers T. C., Stancliffe R. J., 2014, ApJ, 797, 21
Prochaska J. X., 2003, ApJ, 582, 49
Ritter J. S., Safranek-Shrader C., Milosavljević M., Bromm V., 2016, MNRAS, 463, 3354
Romano D., Karakas A. I., Tosi M., Matteucci F., 2010, A&A, 522, A32
Ryan S. G., Aoki W., Norris J. E., Beers T. C., 2005, ApJ, 635, 349
Salvadori S., Ferrara A., 2012, MNRAS, 421, L29
Sharma M., Theuns T., Frenk C., Cooke R., 2016, preprint(arXiv:1611.03868)
Simcoe R. A., Sullivan P. W., Cooksey K. L., Kao M. M., Matejek M. S., Burgasser A. J., 2012, Nature, 492, 79
Simon J. D. et al., 2011, ApJ, 733, 46
Smith B. D., Sigurdsson S., 2007, ApJ, 661, L5
Srianand R., Gupta N., Petitjean P., Noterdaeme P., Ledoux C., 2010, MNRAS, 405, 1888
Stacy A., Bromm V., 2013, MNRAS, 433, 1094
Stacy A., Greif T. H., Bromm V., 2010, MNRAS, 403, 45
Stacy A., Bromm V., Lee A. T., 2016, MNRAS, 462, 1307
Steidel C. C., Strom A. L., Pettini M., Rudie G. C., Reddy N. A., Trainor R. F., 2016, ApJ, 826, 159
Suda T. et al., 2008, PASJ, 60, 1159
Tominaga N., Iwamoto N., Nomoto K., 2014, ApJ, 785, 98
Turk M. J., Abel T., O'Shea B., 2009, Science, 325, 601
Umeda H., Nomoto K., 2003, Nature, 422, 871
Vargas L. C., Geha M., Kirby E. N., Simon J. D., 2013, ApJ, 767, 134
Vogt S. S. et al., 1994, in Crawford D. L., Eric R., Craine E. R., eds., Proc. SPIE Conf. Ser. Vol. 2198, The High-Resolution Echelle Spectrometer on the Keck 10-m Telescope. SPIE, Bellingham, p. 362
Webster D., Bland-Hawthorn J., Sutherland R. S., 2015, ApJ, 804, 110
Wise J. H., Turk M. J., Norman M. L., Abel T., 2012, ApJ, 745, 50
Wolfe A. M., Gawiser E., Prochaska J. X., 2005, ARA&A, 43, 861
Woosley S. E., Weaver T. A., 1995, ApJS, 101, 181
Yuan S., Cen R., 2016, MNRAS, 457, 487

This paper has been typeset from a TEX/LATEX file prepared by the author.